

Weierstraß-Institut für Angewandte Analysis und Stochastik

im Forschungsverbund Berlin e.V.

Preprint

ISSN 0946 – 8633

Profile reconstruction in EUV scatterometry: Modeling and uncertainty estimates

Hermann Gross¹, Andreas Rathsfeld², Frank Scholze¹, and Markus Bär¹

submitted: 13 March 2009

¹ Physikalisch-Technische Bundesanstalt
Abbestr. 2-12
10587 Berlin
Germany
E-Mail: Hermann.Gross@ptb.de
Frank.Scholze@ptb.de
Markus.Baer@ptb.de

² Weierstrass Institute
for Applied Analysis and Stochastics
Mohrenstr. 39
10117 Berlin
Germany
E-Mail: rathsfeld@wias-berlin.de

No. 1411
Berlin 2009



2000 *Mathematics Subject Classification.* 35R30 74J20 35J05.

Key words and phrases. EUV scatterometry, inverse scattering, lithography masks, uncertainty estimates.

The presented investigations are part of the project CDuR32 funded by the Federal Ministry of Education and Research.

Edited by
Weierstraß-Institut für Angewandte Analysis und Stochastik (WIAS)
Mohrenstraße 39
10117 Berlin
Germany

Fax: + 49 30 2044975
E-Mail: preprint@wias-berlin.de
World Wide Web: <http://www.wias-berlin.de/>

Abstract

Scatterometry as a non-imaging indirect optical method in wafer metrology is also relevant to lithography masks designed for Extreme Ultraviolet Lithography, where light with wavelengths in the range of 13 nm is applied. The solution of the inverse problem, i.e. the determination of periodic surface structures regarding critical dimensions (CD) and other profile properties from light diffraction patterns, is incomplete without knowledge of the uncertainties associated with the reconstructed parameters. With decreasing feature sizes of lithography masks, increasing demands on metrology techniques and their uncertainties arise. The numerical simulation of the diffraction process for periodic 2D structures can be realized by the finite element solution of the two-dimensional Helmholtz equation. For typical EUV masks the ratio period over wave length is so large, that a generalized finite element method has to be used to ensure reliable results with reasonable computational costs. The inverse problem can be formulated as a non-linear operator equation in Euclidean spaces. The operator maps the sought mask parameters to the efficiencies of diffracted plane wave modes. We employ a Gauß-Newton type iterative method to solve this operator equation and end up minimizing the deviation of the measured efficiency or phase shift values from the calculated ones. We apply our reconstruction algorithm for the measurement of a typical EUV mask composed of *TaN* absorber lines of about 80 nm height, a period of 420 nm resp. 720 nm, and with an underlying *MoSi*-multilayer stack of 300 nm thickness. Clearly, the uncertainties of the reconstructed geometric parameters essentially depend on the uncertainties of the input data and can be estimated by various methods. We apply a Monte Carlo procedure and an approximative covariance method to evaluate the reconstruction algorithm. Finally, we analyze the influence of uncertainties in the widths of the multilayer stack by the Monte Carlo method.

1 Introduction

An important application of scatterometry is the evaluation of structure dimensions on photo-masks and wafers in lithography [15, 24, 31, 30]. In the semiconductor industry both the feature sizes and the admissible limits of measurement uncertainty decrease continuously. Besides conventional metrology techniques like atomic force, electron and optical microscopy, scatterometry is an important tool for the characterization of such structures [11, 39]. However, scatterometry requires a-priori information. Typically, the surface structure is sought in a certain class of gratings described by a finite number of parameters, and these parameters are confined to certain intervals centered around known design values for the mask under investigation.

The conversion of measurement data into desired geometrical parameters depends crucially on a rigorous modeling by Maxwell's equations [3, 6, 29] and on accurate numerical

algorithms. Note that Maxwell's equations reduce to the two-dimensional Helmholtz equation if geometry and material properties are invariant in one direction. For the numerical solution, a lot of methods have been developed [5, 18, 19, 20, 25, 26, 35]. We use the finite element method (FEM) and truncate the infinite domain of computation to a finite one by coupling with boundary elements [2, 8, 32, 37]. To compute highly oscillatory fields, generalized finite element methods are available [4, 7, 16, 23].

Apart from the forward computations of the Helmholtz equation, the solution of the inverse problem, i.e. the reconstruction of the grating profiles and interfaces from measured diffraction data, is the essential task in scatterometry. This problem is related to the optimal design of diffractive optics [36]. Our approach here employs a Gauß-Newton type iteration [27] proposed e.g. by Al-Assaad and Byrne [1] and is based on FEM computation for the efficiencies of the grating and for derivatives of the efficiencies with respect to the grating parameters [9, 10]. It is well known that the solution of the inverse problem might fail if it is based on insufficient or improper input data. Studies with simulated data for a typical grating representing a photolithographic mask [11] show a strong dependence of the reconstruction result on the subset of efficiencies chosen from the set of all available efficiencies.

There are different methods of sensitivity analysis [12, 14, 21, 22] to find suitable sets of measurement configurations, e.g. convenient angles of incidence or diffraction orders to be measured. The statistical approach is to include as much data as possible but with a weight factor proportional to the reciprocal variance of the individual measurement data. This leads to good results for the inverse reconstruction problem [13]. However, besides the huge amount of measurements, the numerical algorithm converting the measurement data into geometrical parameters becomes computationally more expensive. Hence a smaller set of measurement data may be chosen which is sufficient for a good reconstruction. The sensitivity analysis finds such appropriate sets by minimizing e.g. the condition number of the Jacobian matrix of the mapping from the geometrical parameters to the measurement values [14].

The paper is organized as follows: In Section 2 a brief description of the measurement system for EUV scatterometry will be given. The mathematical formulation of the scattering problem and the numerical algorithms for solving the inverse problem are presented in Section 3. An FEM-based Gauß-Newton type method to solve the reconstruction problem is described and the applied geometrical model for the EUV mask profile is indicated. Section 4 presents the achieved reconstruction results for several measured fields of the EUV mask and discusses their quality. Furthermore, in Section 4 the impact of uncertainties of the measured efficiencies and the influence of stochastically perturbed widths in the underlying multilayer stack to the uncertainties of reconstructed parameters are examined. We will present first estimates for the achievable uncertainty ranges of the reconstructed parameters in dependence on the uncertainties of the input data.

2 Experimental setups: EUV Reflectometer

Scatterometry is known as a collective term for several metrology methods, which may be generally described as measurement techniques for a quantitative evaluation of sur-

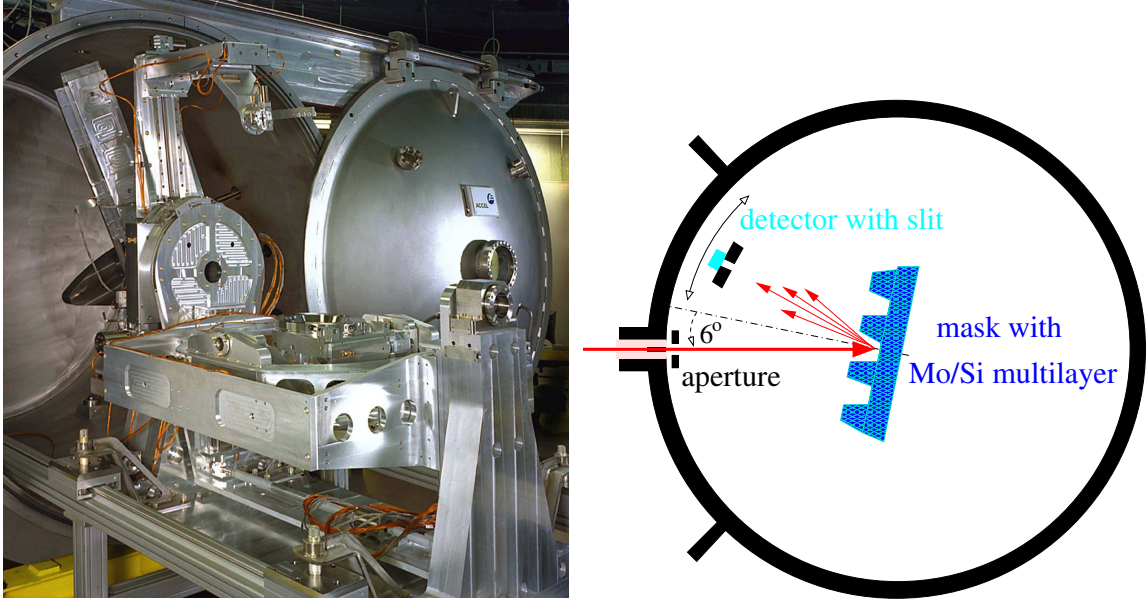


Figure 1: Spectroscopic reflectometer operating in the EUV range (0.7-35nm) and scheme of measurement set-up.

face properties by angle-resolved characterization and analysis of light scattered from a surface under test. Since no imaging optics is used, the surface and shape have to be reconstructed from intensity and/or polarization data detected in the far field. Several measurement modes can be classified as scatterometric techniques, e.g. the standard scatterometer, the spectroscopic reflectometer, the spectroscopic ellipsometer, and the ellipsometric scatterometer.

For the measurements in the EUV range (0.7 - 35 nm wavelength) we use the standard scatterometry approach, i.e. non-specular diffracted light is measured for different wavelengths of the incoming radiation. The measurements are carried out using the EUV reflectometer shown in Fig. 1. The sample under test is an EUV mask with several fields of periodic line-space structures, with different critical dimensions and pitch (period). The absorber stack of the mask consists of three layers, i.e., a thin anti reflection (ARC) layer of (TaO) on top, the main EUV absorber layer (TaN) and a thin buffer layer (SiO_2) which protects the underlying multilayer reflective coating during the manufacturing process of the mask. The reflective multilayer coating beneath these line structures consists of 49 periodically repeated groups of Mo and Si layers. The multilayer is terminated at the surface with a slightly thicker Si -capping layer. In the open reflective areas (spaces between lines), this capping layer is also protected by a thin SiO_2 layer. Fig. 3 shows schematically this design together with some of the most important geometrical parameters. For modelling reasons, the yellow SiO_2 layer is considered to be composed of a layer located beneath the absorber and a layer covering the whole multilayer. The last forms a second capping layer.

3 Model of scatterometry and inverse problem

3.1 Helmholtz equation and its solution

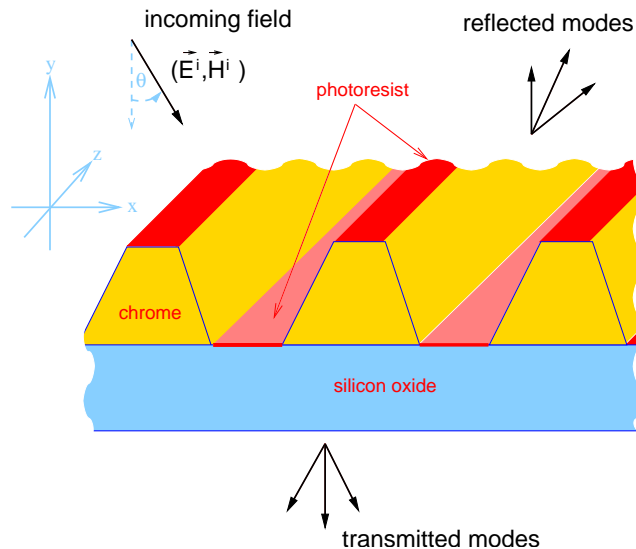


Figure 2: Scheme for wave interaction with a periodic grating structure.

The mathematical basis for modeling the propagation of electromagnetic waves in matter are Maxwell's equations. Their numerical solution represents a direct problem. From the data of the incident light and from characteristic parameters of the irradiated grating, the efficiencies and phase shifts for the different diffraction directions are calculated. Fig. 2 shows a scheme for the irradiation of a periodic surface structure. We use the finite element method (FEM) for the forward calculations on mask profiles. For simplicity, we suppose the direction of the incident wave is in the plane perpendicular to the lines. Since the polarized incident wave can be represented as a superposition of a TE- and a TM-polarized mode, i.e. of waves with the electric field vector oscillating normally and parallel, respectively, to the plane of incidence, Maxwell's equations for the electromagnetic field in the time-harmonic case reduce to the scalar Helmholtz equation over one period of the cross-section domain of the mask specimen (cf. the details in [29, 3]):

$$\Delta u(x, y) + k^2 u(x, y) = 0, \tag{1}$$

Here, the lines of the mask are supposed to be parallel to the y -axis, the plane of incidence is the $x - z$ plane, and the unknown u is the z -component of the electric resp. magnetic field vector. The coefficient $k = k(x, y) = \omega \sqrt{\mu_0 \epsilon(x, y)}$ is the wave number function and ω the angular frequency of the incident light wave. The wave number k is constant in each area of the mask specimen filled by the same material. The FEM solution of this boundary

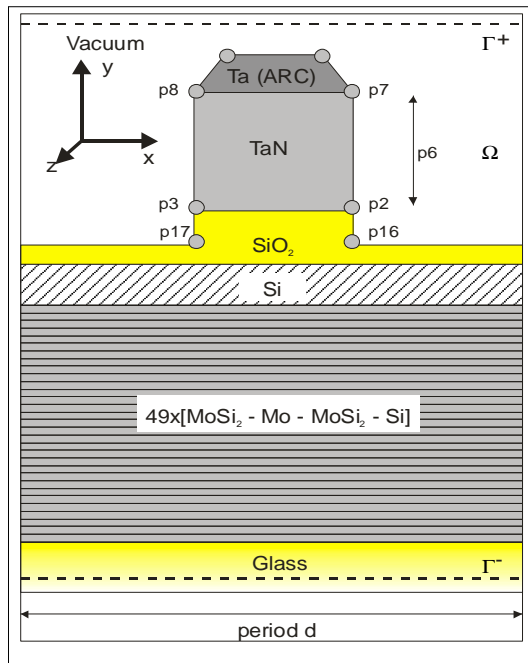


Figure 3: Scheme of an EUV grating structure including the profile parameters to be found.

value problem coupled with the so-called Rayleigh expansion of $u(x, y)$ provides a general solution above and below the mask for the outgoing wave modes. A simple Fourier series expansion of the solution u restricted to lines above the line-space structure gives the coefficients of the reflected plane wave modes. Note that, due to the periodicity of the surface geometry, the far field is the superposition of a finite number of such plane wave modes. Arranging these modes according to the angles of the propagation direction, the plane wave modes can be indexed, and this index is called order of the reflected mode. The ratio of the incoming energy which is radiated into the directions of these plane wave modes is proportional to the squared modulus of their coefficients and is called the efficiency of the mode.

For the approximation accuracy of the FEM the quotient optical wavelength over period of the grating structure is important. If this is markedly smaller than one, e.g. 0.01, then lots of oscillations occur, and either the approximation is poor or the calculation times become unacceptably long. However, by means of a suitable extension of the generalized FEM [4, 16, 23] - as offered by the DIPOG software package [7] - also such cases can be calculated accurately and with reasonable effort.

3.2 Profile reconstruction by optimization

The inverse problem consists in determining the parameters describing the geometry of a certain class of gratings from the measured efficiency/phase shift values. To simplify the notation, we restrict ourselves in the following to efficiency measurements though phase shift measurements can always be included without problem.

Fig. 3 shows a grating class and its geometrical profile model for the cross-section over one period of a typical line-space structure for EUV lithography where the extreme ultraviolet wavelength range is applied. The cross section of the line is a symmetric polygonal domain composed of three trapezoidal layers of different materials (TaO , TaN , and SiO_2). These trapezoids are defined by the heights and by the x -coordinates of the corner points. Beneath the line-space structure there are two capping layers of SiO_2 and of Si followed by a $MoSi$ -multilayer stack (MLS). The last consists of a periodically repeated group of a Mo layer, a Si layers, and two intermediate layers. Note that the MLS is added to enable the reflection of EUV waves. Important geometric profile parameters are, e.g., the height p_6 of the TaN layer (55 - 60 nm) and the x -coordinates relative to the period p_2 and p_7 of the right corners of the TaN layer (e.g. 490/840). In the following evaluations and studies we assume a symmetric profile, i.e., the x -coordinates relative to the period of the corresponding left corner points p_3 resp. p_8 depend on those of the right corner points by $p_3 = 1 - p_2$ and $p_8 = 1 - p_7$. Furthermore we assume a fixed side wall angle (SWA) for the TaO layer of 82.6° representing a certain edge rounding, i.e., the cross-section area of this trapezoidal layer is equal to a corresponding TaO layer having curved upper edges with a radius of about 6 nm. Additionally, we assume that the SWA of the SiO_2 layer should be always equal to the side wall angle of the TaN layer above. For all other model parameters, including the optical indices of the materials and the widths in the capping or the multilayer system, we suppose known values, i.e., they are fixed and will not be sought by our reconstruction method.

To solve the inverse problem an equivalent optimization problem is set up with the following objective functional which is to be minimized:

$$f(\{p_j, j = 1, \dots, J\}) := \sum_{l=1}^L \sum_{m=1}^M \sum_n \omega_n^\pm(\lambda_l, \theta_m) \left[e_n^\pm(\{p_j\}, \lambda_l, \theta_m) - E_n^\pm(\lambda_l, \theta_m) \right]^2, \quad (2)$$

where λ_l , $l = 1, \dots, L$ and θ_m , $m = 1, \dots, M$ are the wavelengths resp. angles of incidence of the measurement, the $E_n^\pm(\lambda_l, \theta_m)$ are the measured efficiencies, and the $\omega_n^\pm(\lambda_l, \theta_m) > 0$ some weight factors. By $e_n^\pm(\{p_j\}, \lambda_l, \theta_m)$ we denote the efficiency of order n for wavelength λ_l and angle of incidence θ_m and for a mask geometry defined by the parameters p_j . If information about the uncertainties of the measured values $E_n^\pm(\lambda_l, \theta_m)$ is available, then it is common and well accepted for least-square procedures to choose the weight factors as the squared reciprocal uncertainties ($\omega_n^\pm(\lambda_l, \theta_m) \propto [u_n^\pm(\lambda_l, \theta_m)]^{-2}$). More precisely, we have

$$f(\{p_j\}) := \chi^2(\{p_j\}) := \sum_{l=1}^L \sum_{m=1}^M \sum_n \frac{1}{[u_n^\pm(\lambda_l, \theta_m)]^2} \left[e_n^\pm(\{p_j\}, \lambda_l, \theta_m) - E_n^\pm(\lambda_l, \theta_m) \right]^2. \quad (3)$$

Applying an iterative algorithm to the optimization of the functional f , the values of the grating parameters are varied until the minimum of the functional has been found. For instance, we can follow the ideas of the Gauß-Newton and of the SQP methods (cf. e.g. [1, 27]). If E is the mapping assigning to the grating parameters $p := \{p_j\}$ the efficiency vector ($e_n^\pm(\{p_j\}, \lambda_l, \theta_m)$), then we look for a solution of $E(p) = E^{meas}$ with $E^{meas} = (E_n^\pm(\lambda_l, \theta_m))$. If p^k is the approximate solution of the k^{th} iteration step, than an improved solution $p^k + \Delta p$ is the solution of

$$E(p^k + \Delta p) \approx E(p^k) + \frac{\partial E}{\partial p}(p^k) \Delta p \approx E^{meas}, \quad \frac{\partial E}{\partial p}(p^k) := \left(\frac{\partial E_m(p^k)}{\partial p_j} \right)_{m,j}.$$

Taking into accounts the upper and lower bounds for the parameters, we arrive at the iteration step $p^{k+1} = p^k + \Delta p$ with Δp the solution of the simple quadratic convex optimization problem with box constraints

$$\min_{\Delta p: p_j^{min} \leq [p^k + \Delta p]_j \leq p_j^{max}} \left\| E(p^k) + \frac{\partial E}{\partial p}(p^k) \Delta p - E^{meas} \right\|^2.$$

The convergence of this method to at least a locally optimal solution can be proved if additional conditions are fulfilled (cf. [14]). In particular a superlinear rate of convergence is possible if a true solution of $E(p) = E^{meas}$ exists. The method is quite fast since no expensive line search step is needed.

To prove the uniqueness of the global minimum solution for the parameter identification of the mask grating structure, seems to be hopeless. However, accurate results will be achieved if there is a sufficiently large number of measured values and if the bounds for the sought parameters have been chosen appropriately. Note that the difficulties with the strong degree of ill-posedness of the inverse reconstruction problem have been overcome by using a priori information to restrict the approximate solution to a class defined by a small number of parameters.

4 Reconstruction results and uncertainty estimates

4.1 Reconstructed results of measured EUV masks

An EUV mask with differently structured fields was measured with the spectroscopic EUV reflectometer already shown in Fig. 1. All measurements were performed for three wavelengths, namely $\lambda_1 = 13.389$ nm, $\lambda_2 = 13.655$ nm, and $\lambda_3 = 13.921$ nm. The orders n of efficiencies with acceptable measurement uncertainties depend on the measured field. For example, in case of a mask field with a ratio line to space of about 1:5 (line width = 140 nm, period = 840 nm) orders from -11 to +11 can be included into the sum for the objective functional (2) resulting in a number of 3×23 measured efficiency values.

A typical example of the objective functional as a function of two grating parameters (layer thickness p_6 and a lateral coordinate p_2) is shown in Fig. 4. The functional was defined choosing the weight factors to be the reciprocal value of the squared uncertainty of the measured efficiencies ($\omega_n^\pm(\lambda_l, \theta_m) \propto [u_n^\pm(\lambda_l, \theta_m)]^{-2}$) and including the diffraction orders from -11 to 11, measured for three different wavelengths and for one angle of incidence (6°). For the selected range of the thickness parameter p_6 two local minima exist. This was to be expected, because the height of the absorber line is very sensitive to interference effects contributing to the reflected wave modes.

Fig. 5 shows the calculated efficiencies for this example, if the optimized profile parameters are used for the simulation. The optimization were executed under the additional constraint that the height p_6 of the *TaN* layer should be greater than 55 nm and smaller than 62 nm. Shown are the simulated efficiencies for λ_1 and λ_2 . They are compared with the measured values and show a fairly good agreement.

If the line to space ratio changes to 1:2 for the same nominal line width of 140 nm, then the measurable efficiencies are smaller and only orders in the range of -6 to +11 can be

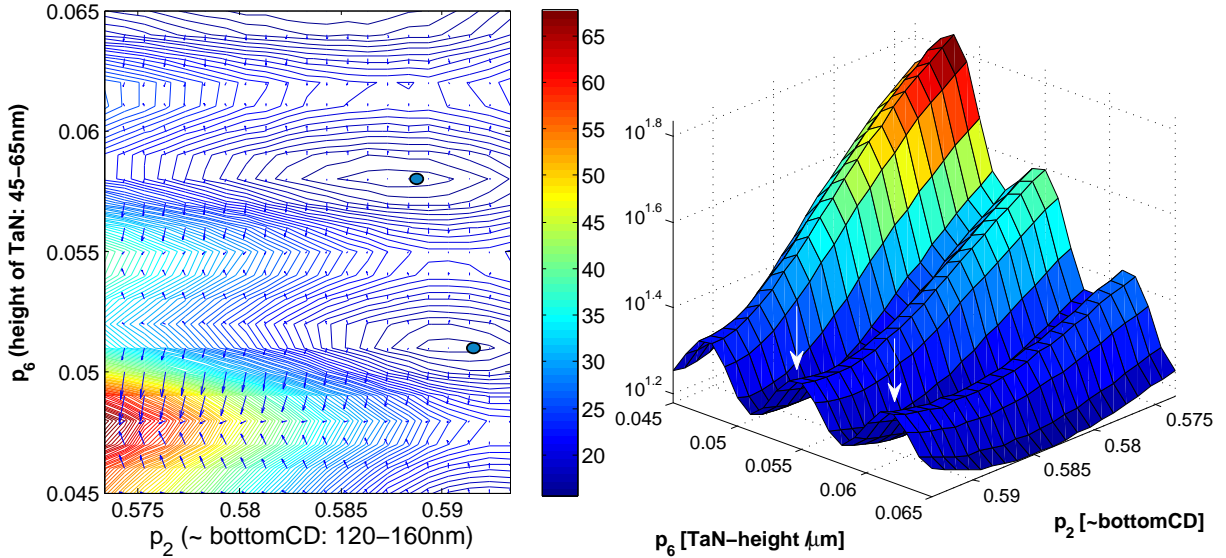


Figure 4: $f = \chi^2$ for a certain field of the EUV mask, shown in dependence on right lower corner point p_2 and height p_6 of the TaN layer (upper right corner fixed); 69 measured efficiencies of orders -11 to +11 over three wavelengths (13.389 nm, 13.655 nm, and 13.921 nm); left as an iso-line and right as surface plot.

measured. Fig. 6 presents the objective functionals for this measurement if the orders from -4 to +4 for λ_1 and λ_2 or -4 to +2 for λ_3 are included in the objective functional. In the considerations in Sect. 4.3 where we will analyze the impact of certain perturbations in the multilayer system, this medium-sized data set of 25 efficiency values will be used. We indicate this by the symbol N2m-25.

In our numerical experiments we choose the weights of the objective functional like in (3) and consider the following simplified statistical model. The uncertainty $u_n^\pm(\lambda_l, \theta_m)$ for the measurement of $E_n^\pm(\lambda_l, \theta_m)$ is the standard deviation of $E_n^\pm(\lambda_l, \theta_m)$ considered as a normally distributed random variable. We assume that the measurements are independent and that there is no systematic error. Moreover, according to measurement experience, the uncertainty $u_n^\pm(\lambda_l, \theta_m)$ can be supposed to be the sum of two independent variables. The first contribution is the background noise of a fixed uncertainty level b_g (typical value of $b_g = 10^{-5} = 0.001\%$), and the second contribution is variable and depends linearly on the mean value $e_n^\pm(\{p_j^{sol}\}, \lambda_l, \theta_m)$. Of course, for simplified and less complicated calculations, the unknown mean value $e_n^\pm(\{p_j^{sol}\}, \lambda_l, \theta_m)$ is replaced by the measured value $E_n^\pm(\lambda_l, \theta_m)$. In other words, we may suppose

$$\left[u_n^\pm(\lambda_l, \theta_m) \right]^2 = \left[a \cdot E_n^\pm(\lambda_l, \theta_m) \right]^2 + b_g^2, \quad (4)$$

where a is a constant factor. Typically the contributions of the detector noise are in the range of 1 - 3% of the measured efficiencies E_n , i.e., $a=0.01$ refers to a noise of 1%. Then, for efficiencies $E_n < 10^{-2}$ the background noise b_g is dominant and the weights become almost independent of E_n .

Table 1 contains the reconstruction results for the measurements at five different fields of the EUV mask. They have all the same nominal line-space ratio of 3:1 at a period of 720 nm and are indicated by $D4$, $H4$, $F6$, $D8$, and $H8$. Because the line to space

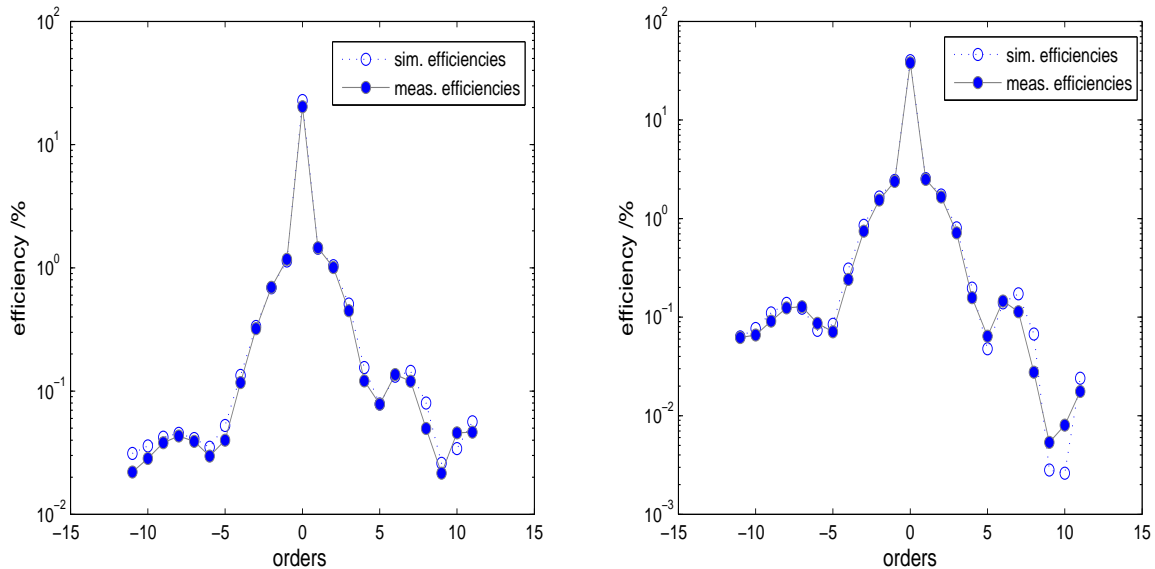


Figure 5: Comparison of measured and calculated efficiencies for one of the optimal solutions for the first two wavelengths ($\lambda_1 = 13.389\text{nm}$, $\lambda_2 = 13.655\text{nm}$).

ratio is increased significantly for these fields of the EUV mask, the number of detectable efficiencies are once again decreased. The optimization was executed for the already discussed profile model of the previous examples (cf. Fig. 3), again imposing symmetrical constraints and using known optical constants for all material components as well as a suitable model (vector of widths for the layers) for the underlying capping and multilayer structure [28, 33]. Instead of the results for the x -coordinates relative to the period of the right corner points p_2 and p_7 the table presents the horizontal width (CD) on the bottom and the top derived from the optimized corner points. Furthermore the height of the TaN layer and the side-wall angle determined from the corner points are indicated.

The model used for the multilayer components, i.e., the widths of the layers, are crucial for such reconstruction results and will be discussed in more detail below. The model was determined by bright-field measurements of special fields on the EUV mask, where only the capping and the multilayer system are present but no absorber lines. At a fixed angle of incidence (6°) the specular reflectance R was measured in dependence on the wavelength changing from 12.8 to 14.4 nm. The evaluation of the layer widths has been performed by the IMD-software for modeling optical properties of thin multilayer structures. Note that IMD allows to take into account rough interfaces by modifying the reflection coefficients of the Fresnel equations [34, 38].

As a test for the results shown in Table 1 the calculated efficiencies (open circles) are compared with the measured ones (closed circles) of field F6 and for the wavelengths λ_1 , λ_2 , and λ_3 used for the measurement. Again a fairly good agreement can be observed in Fig. 7.

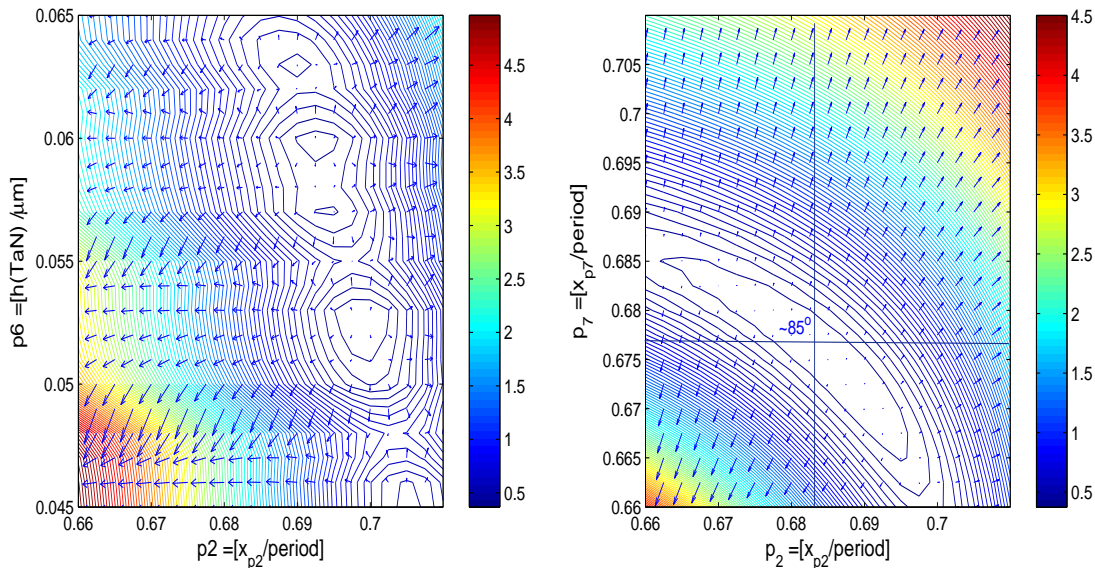


Figure 6: $f(p_2, p_6)$ resp. $f(p_2, p_7)$ for the medium-sized data set N2m-25 of a measured EUV field with a nominal line to space ratio of 1:2 and a period of 420 nm.

field of mask	Bottom CD/nm	Top CD/nm	Height TaN/nm	SWA /°
D4	572.8	540.3	60.52	77.9
H4	623.4	531.9	60.46	57.1
F6	578.8	548.9	60.64	78.9
D8	575.2	538.6	60.86	76.3
H8	575.4	540.7	60.50	77.0

Table 1: Reconstruction results for measurements at five different mask fields with the same nominal values (period: 720 nm, CD: 540 nm). Multilayer parameters used (best approximation from bright-field measurements including roughness): Two capping layers 1.234 nm and 12.869 nm, MLS $49 \times [0.147 \text{ nm} - 2.141 \text{ nm} - 1.972 \text{ nm} - 2.838 \text{ nm}]$.

4.2 Impact of uncertainties in the measurement data

The experimentally measured efficiency values entering the numerical algorithm have an uncertainty. It is important to see how these uncertainties affect the accuracy and the precision of the reconstructed parameter values. To analyze this, we suppose that all the statistical assumptions before Equation (4) are fulfilled and that the uncertainty is given by the relation (4).

First we apply a Monte Carlo method in the spirit of the recommendations in Supplement 1 of the GUM [17] for the determination of uncertainties in measurements, i.e., complete profile reconstructions are repeated many times with randomly perturbed simulated measurement data. So a distribution of the reconstructed parameters is generated and their deviation statistics from the expected values can be calculated. We have studied different sized data sets composed of 12 or 415 efficiencies for reconstructing the profile parameters, i.e., the height of the *TaN* absorber layer in the middle of the line structure, the top

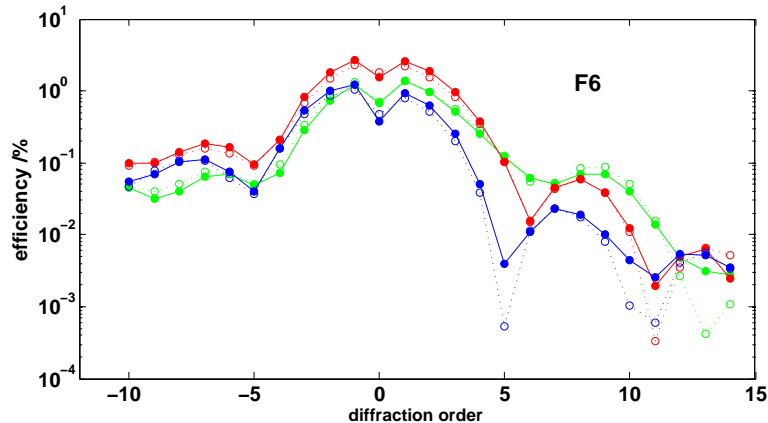


Figure 7: Comparison of measured (closed circles) and simulated (open circles) efficiencies for all three wavelengths of field F6 (green for 13.41 nm, red for 13.68 nm, and blue for 13.94 nm).

and the bottom width. As expected, the range of the distribution of the resulting profile parameters is clearly reduced in the case of substantially larger data sets. However, a 1 nm range is reached already for the smaller data set. Fig. 8 shows the results for the example calculated with 12 efficiencies. The three parameters are labelled here by the indices 6, 7, and 16. The ranges between lower and upper quartiles are indicated by boxes, the medians by lines, and the undisturbed efficiencies by circles. The calculated standard deviations σ_i , $i = 6, 7, 16$, for the reconstructed parameters (layer height and two corner points) are given in nm.

Alternatively, another way to estimate the uncertainties is to follow a proposal by Al-Assaad and Byrne [1]. If the mapping $E : (p_i) \mapsto (e_n^\pm(\{p_j\}, \lambda_l, \theta_m))$ is assumed to be locally almost linear, at least for parameter values (p_i) close to the point of the optimal solution, then the uncertainties of the reconstructed parameters are, again, normally distributed random numbers with zero mean. The standard deviation σ_i of p_i is the square root of the main diagonal entry of the covariance matrix Cov of the parameters, and the latter matrix can be approximated as

$$Cov \approx [J^T \cdot J]^{-1}, \quad J = \left(\frac{\partial E_j}{\partial p_i} \frac{1}{u_j} \right)_{j,i}. \quad (5)$$

That is, the inverse covariance matrix can be approximated by means of the matrix of the partial derivatives of the efficiencies (resp. phase shifts) with respect to the sought parameters, normalized by the uncertainties of the measured data.

If we apply the proposed covariance method to the same numerical examples with simulated measurement data as used for the Monte Carlo method, comparable results are obtained [13]. In fact we observe deviations in the obtained uncertainties of up to 30% for the small and up to 10% for the large data sets. For all parameters investigated and reconstructed with simulated data and even for optimal input data sets of a moderate size, the relative uncertainties have been found to be smaller than 2%. Of course, these

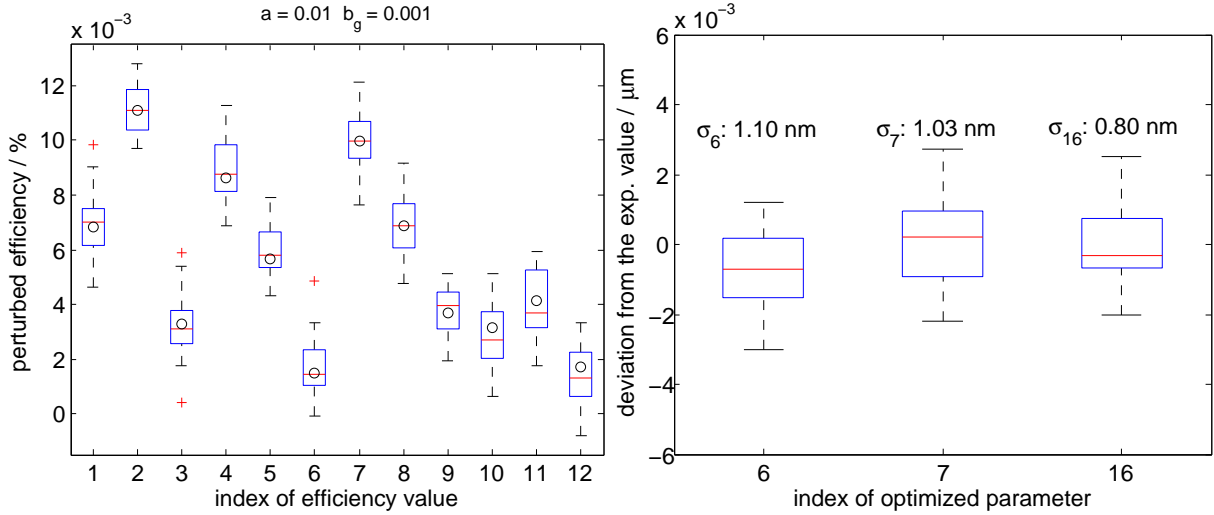


Figure 8: Effect of perturbed simulated efficiencies (left) of a set of 12 values on the deviations of three reconstructed parameters from the expected values and calculated values for σ_6 , σ_7 , and σ_{16} (right) of an EUV mask with a nominal line to space ratio of 1:5 and a period of 840 nm.

results are valid only under the assumption, that the uncertainties resulting from the potential inaccuracies in the geometric modeling of the line-space structure are neglected or are much smaller than the uncertainties resulting from the uncertainties of the measured efficiencies, ranging from 1 to 3% in the numerical examples.

The application of the covariance method to the profile reconstruction of an EUV mask field with a line to space ratio of 1:5 and a period of 840 nm (cf. example in Fig. 4 and 5) yields the results given in Table 2. The standard deviations for the determined corner points, the height of the *TaN* layer, and the side-wall angle SWA are calculated for different noise levels (1%, 3%, and 10%) presumed for the measured efficiencies. Note that the 10% level is not motivated by measurement uncertainties of the efficiencies. Such experiments with large noise are rather meant as a general test for the influence of model parameters with large fluctuations. In fact, so far prescribed model parameters, like e.g. the widths of the MLS, might exhibit larger noise levels.

Data set	N2m-15	N2m-15	N2m-15	N2m-69	N2m-69	N2m-69
noise component a	0.01	0.03	0.10	0.01	0.03	0.10
σ_2 / nm	0.33	0.59	1.70	0.13	0.22	0.58
σ_6 / nm	0.10	0.21	0.65	0.034	0.074	0.20
σ_7 / nm	0.35	0.60	1.70	0.17	0.27	0.62
$\sigma_{\text{SWA}} / ^\circ$	0.46	0.81	2.40	0.21	0.34	0.85

Table 2: Approximated standard deviations determined by the covariance method for two data sets (N2m-15 and N2m-69) with three different noise levels presumed: Reconstruction using efficiency data sets of 15 resp. 69 values; Noise levels of 1%, 3%, and 10% for measured efficiencies give values of σ_2 , σ_6 , σ_7 , and σ_{SWA} ; Background noise 0.001; Line-space ratio 1:5; Period 840 nm.

4.3 Impact of multilayer perturbations

We have already mentioned in the previous sections that the reconstruction results do not only depend on the uncertainties of the measured efficiencies, but on the choice of model parameters too. The capping and multilayer system, determined independently from the parameters of the line-space structure by reconstruction from bright-field measurements, will be shown to be crucial for the final reconstruction of the parameters of the line-space structure. Particularly, effects like perturbations in the widths of the multilayer system beneath the line-space structure are considered.

In order to get assessments about the influence of the MLS and capping parameters on the reconstruction results, we applied a Monte Carlo method. We generate stochastic capping layer/MLS models such that the layer widths are normally distributed independent variables, and consequently, also the total widths of the capping/MLS models are varied. Based on these models, we ran our reconstruction algorithm for the geometric parameters of the line-space structure. Finally, we got the distributions of the sought profile parameters in dependence on the capping layer/MLS models. Fig. 9 presents two examples for perturbed capping layer/MLS models. The reference model with the mean values of the widths for the capping layer/MLS was determined independently by evaluation of bright field reflectance measurements (cf. Section 4.1 and [28]) and is schematically shown in Fig. 3. The distributions in Fig. 9 are achieved by normally distributed fluctuations with 1% for the two capping layers (index 1 and 2) and 1% resp. 0.1% for the *MoSi* group layers of the MLS (index 3 to 4). Recall that the MLS model consist of repeated groups of *Mo* and *Si* layers with intermediate diffusion layers composed of the mixture of both components.

We have examined the noise levels given in the first column of Table 3. Different perturbations for the widths of the capping layers resp. the widths in the MLS allow to separate the impacts of these components. For each of the given fluctuations, the standard deviations of the relative x -coordinates of the corner points p_2 and p_7 as well as that of the height p_6 were calculated. Furthermore the standard deviations σ of the side-wall angles and of the horizontal line widths in the middle of the height of the absorber line, indicated as CDM, were calculated. These parameters are easy to calculate from the reconstructed

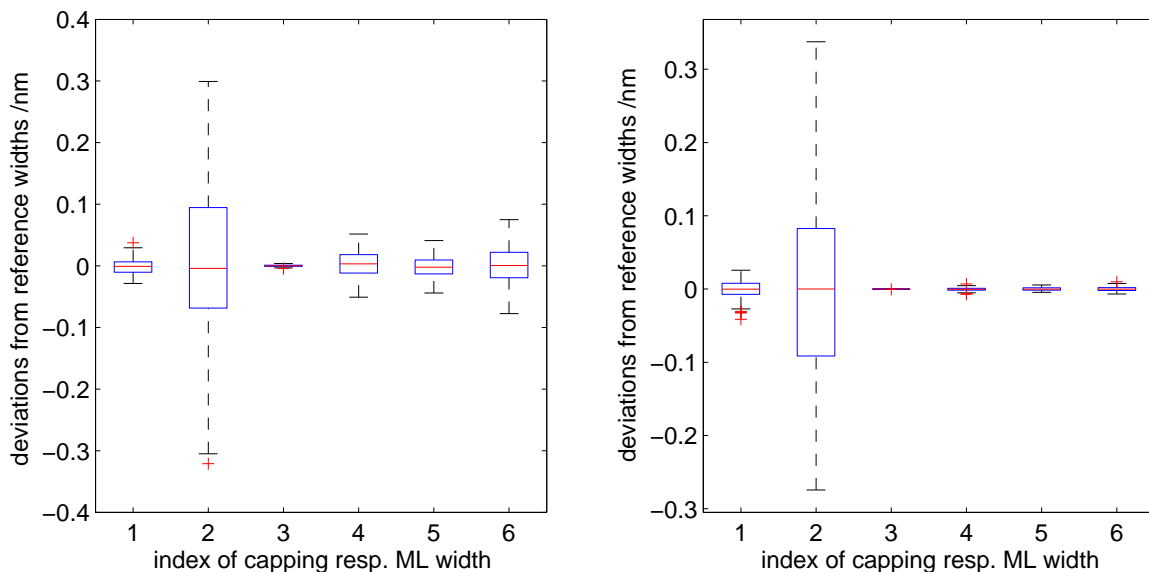


Figure 9: Two examples for distributions of MLS models: Indices 1 to 2 indicate the capping layers; Indices 3 to 6 indicate the four layers of the *MoSi* group of the MLS; Number of samples is 128; left: 1% perturbation of all six parameters; right: 1% resp. 0.1% noise for capping resp. MLS components.

profile parameters p_2 , p_7 , and p_6 . Additionally, the impact of an offset of $\pm 5\%$ for the capping layers relative to the reference model has been studied and the results are given in the last two rows of Table 3.

Figs. 10 and 11 present the details of the generated resp. calculated distributions for one of these examples. Namely, the plots correspond to the case with a noise of 1% in the widths of the capping layers and 0.1% in those of the MLS stack. As already mentioned briefly in Sect. 4.1, for all results presented in Table 3, we have used the medium-sized measurement data set N2m-25 composed of 25 efficiencies. The mask field inspected by the EUV light had a nominal line width of 140 nm and a period of 420 nm corresponding to a line to space ratio of 1:2. For this example, the distributions are shown in Figs. 10 and 11 as statistical box plots with lower and upper quartiles and their median values. The reconstructed profile parameters for the reference values are given in Table 4, and the standard deviations in Table 3 are those of the fluctuation around these reference values.

It is striking to note that for all examined perturbations the standard deviations of the height p_6 of the absorber line are significantly smaller than the deviations for the corner points. This was to be expected due to the higher sensitivity of the height p_6 with respect to the reflected wave modes. We have observed similar results for the standard deviations in dependence on different noise levels of the measured efficiencies (cf. Table 2) in Sect. 4.2. As a consequence of the larger deviations in the horizontal x -coordinates, the standard deviations for the side-wall angles SWA are relatively large and they are always greater than 1.5° . Furthermore it can be observed that, for perturbed MLS widths smaller than 0.5%, the horizontal width at the middle of the height (CDm) has relatively small deviations indicating a stable value. In other words, the reconstruction of CDm is just as stable as that of p_6 .

Perturbation	σ_2 /nm	σ_6 /nm	σ_7 /nm	σ_{SWA} /°	σ_{CDm} /nm
Cap: 1%, MLS: 0.1%	0.86	0.10	0.67	1.52	0.11
Cap: 1%, MLS: 0.5%	1.35	0.29	1.24	2.30	1.19
Cap: 1%, MLS: 1.0%	2.15	0.47	1.79	2.75	2.81
Cap: 2%, MLS: 0.1%	1.21	0.21	0.85	2.06	0.25
Cap: 2% -5% offset, MLS: 0.1%	1.37	0.24	0.81	2.16	0.41
Cap: 2% +5% offset, MLS: 0.1%	0.95	0.36	0.77	1.72	0.17

Table 3: Monte Carlo experiments with perturbed capping layer/MLS models: Applied to reconstruction of measured EUV mask (period 420 nm, line to space ratio 1:2, cf. Fig. 6); Used reference model with capping layer widths of 1.234 nm and 12.869 nm and with an MLS of $49 \times [0.147 \text{ nm}, 2.141 \text{ nm}, 1.972 \text{ nm}, 2.838 \text{ nm}]$.

Data set	$p_2 - p_3$ /nm	p_6 /nm	$p_7 - p_8$ /nm	SWA /°	CDm /nm
N2m-25	157.7	57.19	143.1	85.0	150.92

Table 4: Reconstructed parameters for the measurement values of the medium-sized data set (N2m-25): Period 420 nm, line to space ratio 1:2, capping layer widths [1.234 nm, 12.869 nm], MLS widths $49 \times [0.147 \text{ nm}, 2.141 \text{ nm}, 1.972 \text{ nm}, 2.838 \text{ nm}]$.

An offset of $\pm 5\%$ for the widths of capping layers (cf. last two rows of Table 3) does not affect significantly the standard deviations of the reconstructed parameters. However, a systematic shift of the reconstructed side-wall angle SWA appears. In fact, the side-wall angle increases significantly if the widths of the SiO_2 and Si capping layers are presumed to be smaller than the corresponding references values 1.234 nm and 12.869 nm. In Fig. 12 this increase is manifested by the significant shifts of the median values for σ_2 and σ_7 to the negative and positive direction, respectively. The mean side-wall angle increases to 87.8° compared with 85.0° for the reference thickness values. The side-wall angle measured by atomic force microscopy is between 86.9° and 87.6° .

If we pick up the thickness of the first capping layer, i.e., the SiO_2 layer, and perform the optimization of our reconstruction algorithm to get the relative x -coordinates of the lower and upper corner points in dependence on the varying thickness of the first capping layer, then again a strong correlation of the resulting side-wall angle is exhibited in Fig. 13.

5 Summary and conclusions

To solve the reconstruction problem for EUV scatterometry by 2D line structures, we have proposed a trapezoidal shaped profile model composed of different material components and parameterized by the relative x -coordinates of the corner points and by the heights. The inverse problem has been formulated as a non-linear operator equation which includes the mapping of the vector of sought parameters to the vector of certain efficiencies of the plane-wave modes diffracted by the mask. An FEM based Gauß-Newton type method has been applied to solve the operator equation reformulated as an optimization problem.

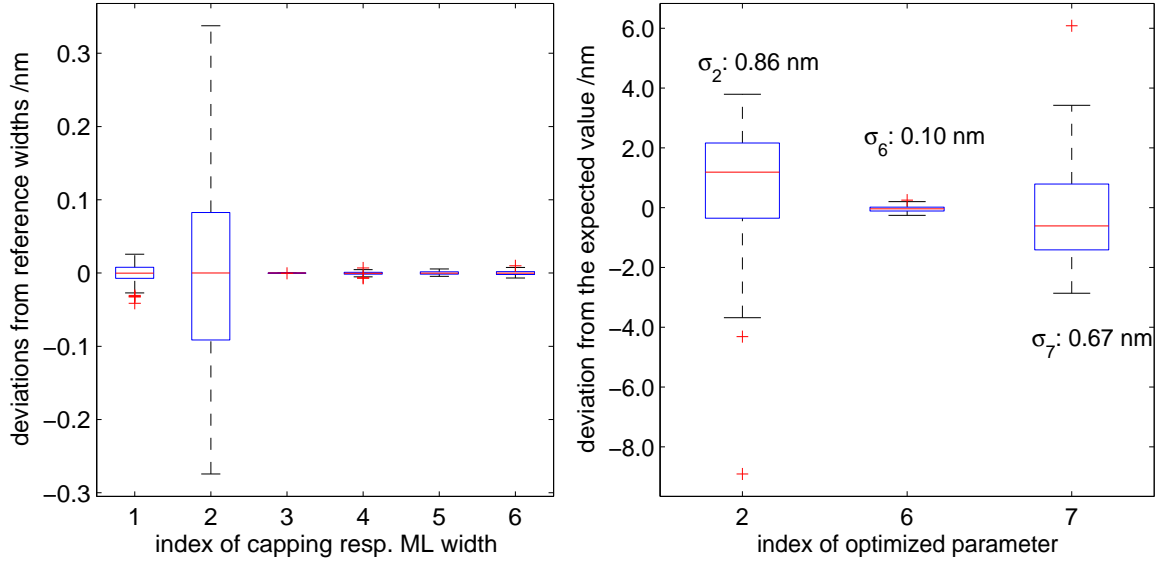


Figure 10: Distributions of capping layer and MLS widths (left, noise for capping widths 1% resp. noise for MLS widths 0.1%) and their impact to the reconstructed profile parameters (right, 112 samples).

If the number of measured values is sufficiently large and if the bounds for the sought parameters are chosen appropriately, precise results can be achieved for EUV masks with different line to space ratios (1:5,1:2,3:1) and with different periods (840 nm, 420 nm, 720 nm). For the sake of simplicity, we have restricted our examinations to a symmetric profile model, where only three important parameters are sought, namely, the two relative x -coordinates of the lower resp. the upper right corners of the layer in the middle of the line structure and the thickness of this layer.

Clearly the uncertainties of the reconstructed parameters depend on the uncertainties of the input data for the reconstruction algorithm. Firstly, we have analyzed the impact of normally perturbed efficiencies for different-sized measurement data sets by a Monte Carlo method and, additionally, by an approximate covariance matrix method. If the relative uncertainties of the measured efficiencies are about 1%, then the relative uncertainties of the reconstructed parameters have been found to be smaller than 2%. This holds even for input data sets of moderate size and for the reconstruction of the side-wall angle.

Secondly, we have analyzed the influence of certain presumed and fixed model parameters, namely, the thicknesses of the two capping layers and the four widths in the periodically repeated groups of the multilayer system. We have confined our tests to a single medium-sized data set and to the Monte Carlo method. Applying Monte Carlo method means, stochastically perturbed thicknesses with normal distributions have been inserted into the capping resp. MLS model, and reconstructions for all these perturbed models have been performed to determine the statistics of the reconstructed parameters of the line-space structure. It has turned out, that the impact of such model based uncertainties is crucial: The CD for the bottom and the top of the line structure show significantly increased variations. Even for the smallest presumed perturbation (capping layer thickness perturbed by 1% and MLS layers by 0.1%), the standard deviation of the side-wall angle

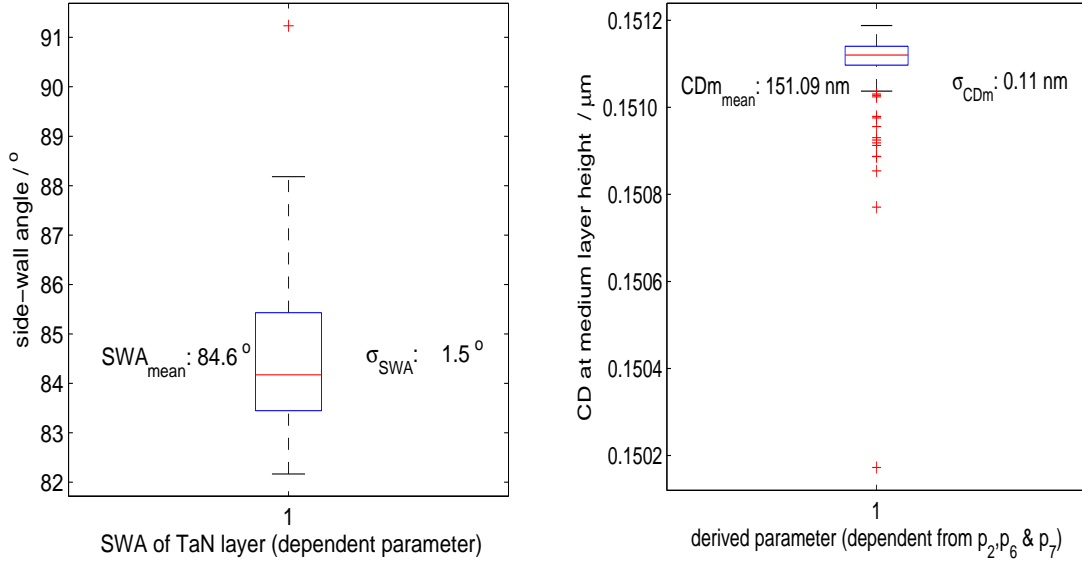


Figure 11: Distribution of side-wall angles (left) and horizontal line widths in the middle of the height (right) of the line structure (noise for capp. widths 1% resp. 0.1% for ML widths; 112 samples).

σ_{SWA} is greater than 1.5° . On the other hand, we have observed that the height of the line-space structure and its mean CD are relatively stable with respect to the model based uncertainties. Furthermore, our examinations have revealed a strong correlation between the thicknesses of the capping layers, e.g. the SiO_2 layer, and the side-wall angle.

The estimation of total measurement uncertainty of the reconstructed profile parameters was not the objective of the presented investigations. The Monte Carlo method has to be applied simultaneously to all relevant input data of the inverse problem to determine the overall measurement uncertainty, as described in Supplement 1 of the GUM [17]. This will be studied in further investigations. Instead, we can infer a first estimate for the impact of certain model uncertainties, e.g. the fluctuation in the thicknesses of the capping layers and the MLS. It leads to a rise in the uncertainties of up to 3% for all parameters investigated and is thus at least comparable to the detector-noise related uncertainties. Future work will deal with further model imperfections and the impact of roughness at the layer interfaces is supposed to be the most important one.

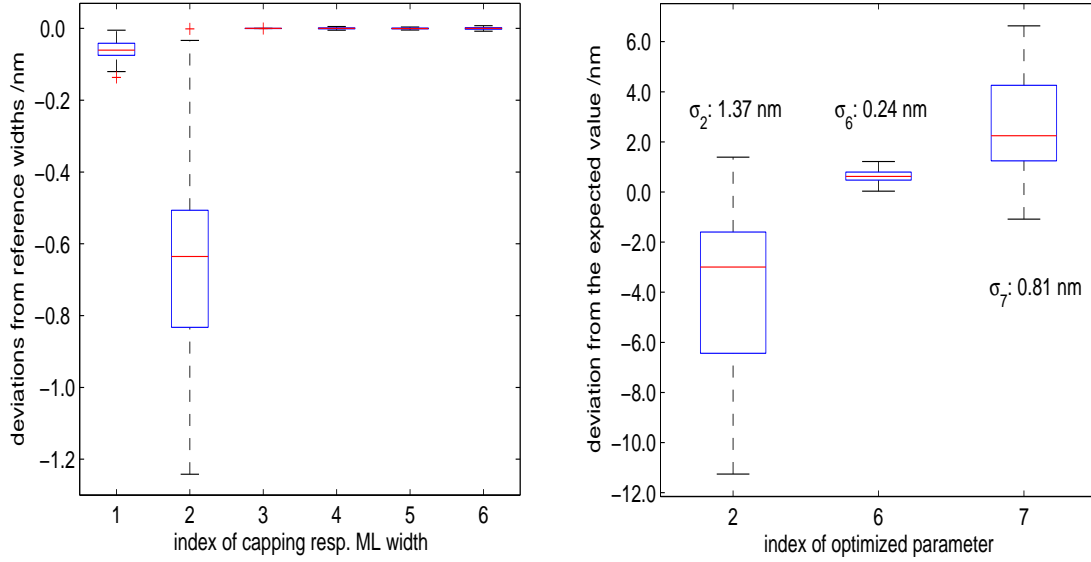


Figure 12: Left: Distribution of capping layer widths, imposed with an offset of -5% and a noise of 2%, and MLS widths with a noise of 0.1%. Right: Impact of these perturbations to the reconstructed profile parameters (97 samples).

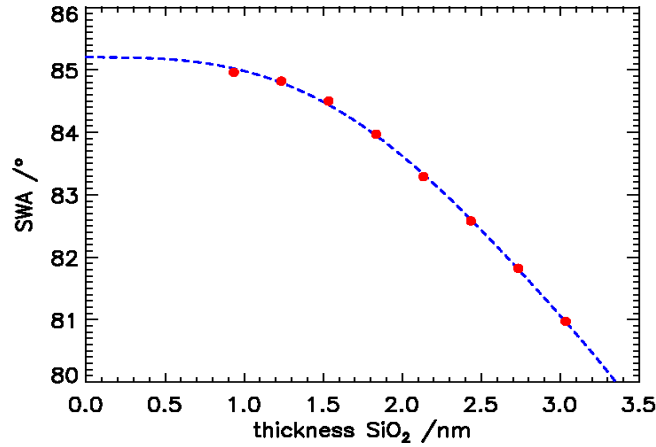


Figure 13: Dependence of reconstructed side-wall angle on thickness of *SiO₂* capping layer: Measurements for a mask field with line-space ratio of 1:2 and with a period of 420 nm.

References

- [1] Alassaad, R.M. and Byrne, D.M., “Error Analysis in Inverse Scatterometry I: Modeling”, *JOSA A*, **24**, pp. 326–338, 2007.
- [2] Bao, G., “Finite element approximation of time harmonic waves in periodic structures”, *SIAM J.Numer.Anal.*, **32**, pp. 1155–1169, 1995.
- [3] Bao, G. and Dobson, D.C., “Modeling and optimal design of diffractive optical structures”, *Surveys on Mathematics for Industry*, **8**, pp. 37–62, 1998.
- [4] Cessenat, O. and Depres, B., “Application of an ultra weak variational formulation of elliptic PDEs to the two-dimensional Helmholtz problem”, *SIAM J.Numer.Anal.*, **35**, pp. 255-299, 1998.
- [5] Chandezon, J., Maystre, D., and Raoult, G., “A new theoretical method for diffraction gratings and its applications”, *J.Opt. (Paris)*, **11**, pp. 235–241, 1980.
- [6] Chen, X. and Friedmann, A., “Maxwell’s equation in a periodic structure”, *Trans. Amer. Math. Soc.*, **323**, pp. 811–818, 1991.
- [7] Elschner, J., Hinder, R., Rathsfeld, A., and Schmidt, G., internet *DIPOG Homepage*, <http://www.wias-berlin.de/software/DIPOG>.
- [8] Elschner, J., Hinder, R., and Schmidt, G., “Finite element solution of conical diffraction problems”, *Advances in Comp.Math.*, **16**, pp. 139–156, 2002.
- [9] Elschner, J. and Schmidt G., “Conical diffraction by periodic structures: Variation of interfaces and gradient formulas”, *Math.Nachr.*, **252**, pp. 24–42, 2003.
- [10] Elschner, J. and Schmidt, G., “Numerical solution of optimal design problems for binary gratings”, *J.Comput.Physics*, **146**, pp. 603–626, 1998.
- [11] Gross, H., Model, R., Bär, M., Wurm, M., Bodermann, B., and Rathsfeld, A., “Mathematical modelling of indirect measurements in scatterometry”, *Measurement*, **39**, pp. 782-794, 2006.
- [12] Gross, H., Rathsfeld, A., Scholze, F., Bär, M., and Dersch, U., “Optimal sets of measurement data for profile reconstruction in scatterometry”, *Proc. of SPIE*, **6617**, pp. 1B1-1B12, 2007.
- [13] Gross, H., Rathsfeld, A., Scholze, F., Model, R., and Bär, M., “Computational methods estimating uncertainties for profile reconstruction in scatterometry”, *Proc. of SPIE*, **6995**, pp. 0T1-0T9, 2008.
- [14] Gross, H. and Rathsfeld, A., “Sensitivity analysis for indirect measurement in scatterometry and the reconstruction of periodic grating structures”, *Waves in Random and Complex Media*, **18**, No.1, pp. 129-149, 2008.

- [15] Huang, H.T. and Terry Jr., F.L., Erratum to “Spectroscopic ellipsometry and reflectometry from gratings (Scatterometry) for critical dimension measurement and in situ, real-time process monitoring” [Thin Solid Films 455-456 (2004) 828-836], *Thin Solid Films*, **468**, pp. 1155–1169, 2004.
- [16] Ihlenburg, F., *Finite element analysis of acoustic scattering*, Springer Verlag New-York, Berlin Heidelberg, Applied Mathematical Sciences **132**, 1998.
- [17] Joint Committee for Guides in Metrology, “BIPM, IEC, IFCC, ILAC, ISO, IUPAC, IUPAP, and OIML. Evaluation of measurement data – Supplement 1 to the ”Guide to the expression of uncertainty in measurement” – Propagation of distributions using a Monte Carlo method.”, Bureau International des Poids et Mesures, JCGM 101, 2008.
- [18] Kleemann, B.H., *Elektromagnetische Analyse von Oberflächengittern von IR bis XUV mittels einer parametrisierten Randintegralmethode: Theorie, Vergleich und Anwendungen*, Dissertation, TU Ilmenau, 2002, Mensch und Buch Verlag Berlin, 2003.
- [19] Lalanne, P. and Morris, G.M., “Highly improved convergence of the coupled-wave method for TM-polarization”, *JOSA A*, **13**, pp. 779–784, 1996.
- [20] Li, L., “New formulation of the Fourier modal method for crossed surface-relief gratings”, *JOSA A*, **14**, pp. 2758–2767, 1997.
- [21] Logofatu, P. C., “Sensitivity analysis of grating parameter estimation”, *App. Optics*, **41**, pp. 7179-7186, 2002.
- [22] Logofatu, P. C., “Phase-modulation scatterometry”, *App. Optics*, **41**, pp. 7187-7192, 2002.
- [23] Melenk, J.M. and Babuška, I., “The partition of unity method: Basic theory and applications”, *Comp.Methods Appl.Mech.Eng.*, **139**, pp. 289–314, 1998.
- [24] Minhas, B.K., Coulombe, S.A., Sohail, S., Naqvi, H., and McNeil, J.R., “Ellipsometric scatterometry for metrology of sub-0.1 μm -linewidth structures”, *Appl. Optics*, **37**, No. 22, pp. 5112–5115, 1998.
- [25] Moharam, M.G. and Gaylord, T.K., “Rigorous coupled wave analysis of planar grating diffraction”, *J.Opt.Soc.Amer.*, **71**, pp. 811–818, 1981.
- [26] Moharam, M.G., Grann, E.B., Pommet, D.A., and Gaylord, T.K., “Stable implementation of the rigorous coupled-wave analysis for surface-relief gratings: enhanced transmittance matrix approach”, *JOSA A*, **12**, pp. 1077–1086, 1995.
- [27] Nocedal, J. and Wright, S.J., *Numerical optimization*, Springer Verlag New-York Berlin Heidelberg, Springer Series in Operation Research, 2000.
- [28] Perlich, J., Kamm, F.-M., Rau, J., Scholze, F., and Ulm, G., “Characterization of extreme ultraviolet masks by extreme ultraviolet scatterometry”, *J. Vac. Sci. Technol.*, **B22**, pp. 3059-3062, 2004.
- [29] Petit, R. (ed.), *Electromagnetic theory of gratings*, Springer-Verlag Berlin, 1980.

- [30] Raymond, C.J., Murnane, M.R., Prins, S.L., Sohail, S., Naqvi, H., and McNeil, J.R., “Multiparameter grating metrology using optical scatterometry”, *J. Vac.Sci. Technol.*, **15** (2), pp. 361–368, 1997.
- [31] Raymond, C.J., Murnane, M.R., Sohail, S., Naqvi, H., and McNeil, J.R., “Metrology of subwavelength photoresist gratings using optical scatterometry”, *J. Vac.Sci. Technol.*, **13** (4), pp. 1484, 1995.
- [32] Schaedle, A., Zschiedrich, L., Burger, S., Klose, R., and Schmidt, F., *Domain decomposition method for Maxwell’s equations: Scattering of periodic structures*, ZIB-Report 06-04, Konrad Zuse Institut, Berlin, 2006.
- [33] Scholze, F., Laubis, C., Dersch, U., Pomplun, J., Burger, S., and Schmidt, F., “The influence of line edge roughness and CD uniformity on EUV scatterometry for CD characterization of EUV masks”, *Proc. of SPIE*, **6617**, 2007, 1A1-1A10.
- [34] Stearns, D. G., “The scattering of x rays from nonideal multilayer structures”, *J. Appl. Phys.*, **65** (2), pp. 491-506, 1989.
- [35] Tavrov, A., Totzeck, M., Kerwien, N., and Tiziani, H.J., “Rigorous coupled-wave analysis calculus of submicrometer interference pattern and resolving edge position versus signal-to-noise ratio”, *Opt.Eng.*, **41** (8), pp. 1886–1892, 2002.
- [36] Turunen, J. and Wyrowski, F. (eds.), *Diffraction Optics for Industrial and Commercial Applications*, Akademie Verlag, Berlin, 1997.
- [37] Urbach, H.P., “Convergence of the Galerkin method for two-dimensional electromagnetic problems”, *SIAM J.Numer.Anal.*, **28**, pp. 697–710, 1991.
- [38] Windt, D. L., “IMD-Software for modeling the optical properties of multilayer films”, *Computers in Physics*, **12** (4), 1998, 360-370.
- [39] Wurm, M., Bodermann, B., and Mirandé, W., “Evaluation of scatterometry tools for critical dimension metrology”, *DGaO Proceedings*, **106**, 2005.